Modeling optoelectronic oscillators

Etgar C. Levy,[1,*] Moshe Horowitz,[1] and Curtis R. Menyuk[2]

[1]*Department of Electrical Engineering, Technion-Israel Institute of Technology, Haifa 32000, Israel*
[2]*Department of Electrical Engineering, University of Maryland, Baltimore, Maryland 21250, USA*
*Corresponding author: etgarlevy@gmail.com

We have developed a comprehensive simulation model for accurately studying the dynamics in optoelectronic oscillators (OEOs). Although the OEO is characterized by three widely separated time scales, our model requires neither long run times nor a large amount of memory storage. The model generalizes the Yao–Maleki model and includes all of the physical effects in the Yao–Maleki model as well as other physical effects that are needed to calculate important features of the OEO dynamics, such as the impact of the fast response time of the modulator on the phase noise power spectral density, the fluctuations of the OEO output due to the input noise, the cavity mode competition during the OEO start-up, and temporal amplitude oscillations in steady state. We show that the absolute value of the phase noise is 2−3 dB lower than predicted by the Yao–Maleki model. The Yao–Maleki model does not take into account amplitude noise suppression due to the fast time response of the modulator, which accounts for this difference. We show that a single cavity mode oscillates in the OEO at steady state, and this mode is determined by the noise that is present when the OEO is turned on. When the small-signal open-loop gain is higher than 2.31, we show that the OEO amplitude oscillates in steady state. This temporal amplitude oscillation can be suppressed by using a narrow filter. Our simulation model, once extended to include flicker $(1/f)$ noise and different amplifier and modulator designs, will enable its users to accurately design OEOs. © 2008 Optical Society of America

OCIS codes: 060.2320, 230.0250, 230.4910.

1. INTRODUCTION

Optoelectronic oscillators (OEOs) were invented by Yao and Maleki in 1996 [1,2]. Traditional RF oscillators that operate in the neighborhood of tens of gigahertz are based on frequency multiplication of a low-frequency reference, such as a quartz oscillator [3]. Since the required multiplication factor of the low-frequency reference source is high, such devices have a relatively high phase noise [3]. Due to the low loss of optical fibers, the cavity length of OEOs can be of the order of a few kilometers. Such cavities have a high Q that can be as large as 10^{10}, and hence the phase noise that is obtained can be far lower than can be obtained using traditional RF oscillators. Moreover, in contrast to traditional RF oscillators, the phase noise in OEOs is independent of the oscillation frequency [3].

The cavity length of OEOs is sufficiently long to make the cavity mode spacing smaller than the bandwidth of the intracavity RF filter. Therefore, the output of the OEO may contain spurs that are not acceptable in RF systems. Several OEO configurations such as the dual-loop OEO [4,5], the mutually coupled OEOs [6], the coupled OEO (COEO)[7], and the injection-locked dual OEO [8,9], based on using two or more cavities have been developed in an attempt to reduce the spurs. Using a dual injection-locked OEO in a master–slave configuration, Zhou and co-workers [8,9] have demonstrated a spur level that is better than −140 dBc/Hz and a phase noise that is close to −100 dBc/Hz at a frequency offset of 70 Hz from the carrier frequency. However, even such an excellent performance may be insufficient for important applications such as Doppler radar [10].

A simple model for analyzing the time-averaged noise in OEOs was developed by Yao and Maleki [2]. The theoretical dependence of the time-averaged phase noise on the frequency offset from the carrier frequency, the cavity length, and the oscillation power were verified experimentally [2]. The Yao–Maleki model is only concerned with the final steady state of the OEO and assumes that the signal at any point in the OEO, both in the optical and RF domains, does not depend on time. Thus, this model cannot be used to study the start-up from noise and does not enable one to take into account dynamical effects such as noise fluctuations, mode hopping between cavity modes, or temporal amplitude oscillations. These effects have been observed to degrade the performance of OEOs in some operating regimes. Moreover, the Yao–Maleki model cannot take into account non-white-noise sources. Experimental results indicate that flicker noise $(1/f$ or pink noise) plays a significant role in OEOs [5].

It is therefore of great importance to generalize the Yao–Maleki model to include these additional physical effects. Systematically identifying and then eliminating or reducing these effects could lead to a dramatic improvement in the performance of OEOs. Given the large size of the parameter space to be explored it is necessary to use an efficient yet accurate computational model that is capable of predicting the OEO behavior over the entire frequency and parameter range of interest. Such a model should enable its users to find parameter regimes where dynamical effects are suppressed and to determine the ultimate phase-noise limits in OEOs. The model should be easily generalizable to allow its users to explore the impact of different device and noise characteristics.

Developing a computational model of the OEO that in-

cludes the important dynamical effects is a challenging task since the OEO is characterized by three widely separated time or frequency scales. The highest frequency scale, of the order of few gigahertz, is the frequency of the output signal. The second frequency scale, of the order of hundreds of kilohertz, is the cavity mode spacing. The last frequency scale, of the order of several to thousands of hertz, corresponds to the frequency of the phase noise that is of interest. Strictly speaking, there is another fourth frequency scale, of the order of 100 THz, that corresponds to the carrier frequency of the light in the OEO's optical fiber. However, it appears merely as the carrier of the signal and has no effect on the computational model.

A model for studying the signal dynamics in OEOs has been developed by Chembo *et al.* [11] that is based upon a delay-differential equation. This model makes a number of simplifying assumptions. The most important of these assumptions are: (1) The cavity mode spacing is small compared with the bandwidth of the filter and the amplifier. (2) Both the signal variation at the modulator and along the cavity are small, so that the order of the components does not affect the round-trip signal transmission. These assumptions are incorrect when the cavity mode spacing is comparable to the filter bandwidth. In particular, one cannot use this model to accurately calculate the spurious level when the filter bandwidth is narrow.

In this paper, we describe a new, comprehensive simulation model of a single-loop OEO. The model includes all the physical effects in the Yao–Maleki model as well as additional physical effects such as the fast response time of the modulator, the ability of the OEO to oscillate in several cavity modes, and signal fluctuations that are induced by the input noise. These effects are required to model the dynamics in OEOs. Our model requires neither a large amount of memory storage nor long run times. It can be easily modified to include different device and noise characteristics. We have calculated the time-averaged phase noise with an additive white Gaussian noise source using our model and compared it to the results of the Yao–Maleki model. Both models yield the same dependence of the average phase noise on the cavity length, the oscillating power, and the carrier offset frequency that was verified in previous experiments [2]. However, our model predicts that the phase noise is 2 to 3 dB lower than is predicted by the Yao–Maleki model when the small-signal open-loop gain is greater than about 1.5. This discrepancy is due to the fast response time of the modulator. This effect, which is not included in the Yao–Maleki model, suppresses most of the amplitude noise in OEOs. Complete amplitude noise suppression in OEOs would yield a 3 dB difference between the magnitude of the RF spectrum calculated by the two models, but the suppression is incomplete.

We have studied the oscillation start-up from additive white Gaussian noise and we have found that several different cavity modes simultaneously oscillate when the cavity mode spacing is smaller than the filter bandwidth. However, one cavity mode whose frequency is randomly determined by the initial noise eventually wins the mode competition. Once the OEO reaches steady state, we have observed no mode hopping between cavity modes, indicat-

ing that experimentally observed mode hopping [12] is not due to additive Gaussian white noise and must be due to flicker ($1/f$ or pink) noise that is from the amplifiers or environmentally driven changes in fiber length.

We have studied the steady-state OEO dynamics, and we have observed that the amplitude of the steady-state cavity mode oscillates when the small-signal open-loop gain $G_S \gtrsim 2.31$ and the RF filter bandwidth is greater than $2/\tau$ where τ is the round-trip time. We explain this threshold value using a simple physical argument. Chembo *et al.* [11] have experimentally observed these oscillations and theoretically explained them using a delay-differential equation. However, the threshold that they derive for the amplitude oscillation does not include the effect of the filter bandwidth.

When $G_S \gtrsim 2.9$ and the filter bandwidth $\Gamma \gtrsim 2/\tau$, the amplitude of the steady-state cavity mode oscillates with more than one frequency, leading to an aperiodic evolution in time.

Modern-day OEOs are becoming increasingly complex. They are typically designed with multiple loops, and a variety of different configurations are possible. One must also choose between several different amplifier designs and the different noise sources, such as white noise, flicker noise from the amplifiers, and flicker noise from environmentally driven changes in the fiber length, all may play an important role in different parameter regimes. The development of a comprehensive simulation model that can be used to study these devices has become imperative and in this paper we present such a model. We present the basic model and simple, yet important, applications to single-loop OEOs that allow us to compare our model to the earlier theoretical work of Yao and Maleki [2] and Chembo *et al.* [11], while at the same time serving as a departure point and basis of comparison for studying more complex systems in the future.

The remainder of this paper is organized as follows. In Section 2 we present the simulation model. In particular we describe the multiple scale approach that we use. This approach allows us to successfully follow the three widely disparate time scales that must be simulated. In Section 3 we present the application of our model to the calculation of the phase noise power spectral density, to the study of the start-up process, and to the determination of the threshold for amplitude oscillations in steady state. These applications are all made within the relatively simple context of single-loop OEOs, which allows us to connect our results to the earlier theoretical work of Yao and Maleki [2] and Chembo *et al.* [11]. Finally, Section 4 contains the conclusions.

2. OPTOELECTRONIC OSCILLATOR MODEL

The OEO configuration analyzed in this paper is shown schematically in Fig. 1. The configuration is identical to that studied theoretically and experimentally in [1–3]. Light from a laser is fed into an electro-optic (E/O) modulator, which is used to convert microwave oscillations into a modulation of the light intensity. The modulated light is sent through a long fiber and is then detected using a photodetector. The photodetector converts the modulated
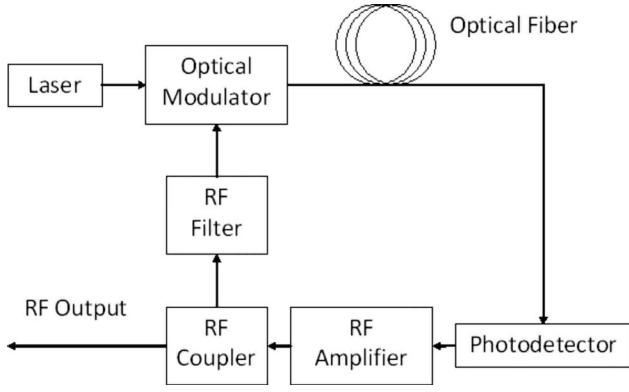
Fig. 1.   Schematic of the OEO.

light signal into an electrical signal. The output electrical signal is amplified, filtered, and fed back into the electrical port of the modulator.

Since in experiments the bandwidth of the RF filter, Γ, as well as the bandwidth of the electrical amplifier are significantly narrower than the central frequency ω_c, i.e., $\Gamma \ll \omega_c$, the bandwidth of the generated signal is limited. Hence, we assume that the voltage applied to the modulator, $V_{\mathrm{in}}(t,T)$, is approximately a sinusoidal wave with an angular carrier frequency ω_c, a time dependent phase $\phi(T)$, and a time dependent amplitude $|a_{\mathrm{in}}^{\mathrm{mod}}(T)|$, so that

$$V_{\mathrm{in}}(t,T) = |a_{\mathrm{in}}^{\mathrm{mod}}(T)|\cos[\omega_c t + \phi(T)]$$

$$= \frac{1}{2} a_{\mathrm{in}}^{\mathrm{mod}}(T)\exp(-i\omega_c t) + \mathrm{c.c.}, \qquad (1)$$

where the angular carrier frequency, ω_c, is of the order of $2\pi \times 10$ GHz; t is a fast time scale of the order of $2\pi/\omega_c \approx 100$ ps; T is a slow time scale of the order of the round-trip time $T \approx 10$ μs; and $a_{\mathrm{in}}^{\mathrm{mod}}(T) = |a_{\mathrm{in}}^{\mathrm{mod}}(T)|\exp[-i\phi(T)]$ is the complex envelope or the phasor of the voltage $V_{\mathrm{in}}(t,T)$. We assume that $d\phi/dT \ll \omega_c$ and that $d|a_{\mathrm{in}}^{\mathrm{mod}}|/dT \ll |a_{\mathrm{in}}^{\mathrm{mod}}|\omega_c$.

The optical power at the output port of the E/O modulator is related to the input electrical signal by a nonlinear transfer curve. The nonlinearity in the E/O modulator generates harmonic components at frequencies $m\omega_c$ where m is an integer. The optical power from the E/O modulator is converted to an electric signal by a photodetector and is then amplified using an electrical amplifier. The relation between the output electrical signal of the RF amplifier and the input electrical signal of the modulator V_{in} may be written [2] as

$$V_{\mathrm{out}}(t,T) = V_{\mathrm{ph}}(1 - \eta\sin\{\pi[V_{\mathrm{in}}(t,T)/V_\pi + V_B/V_\pi]\}), \quad (2)$$

where V_π is the modulator half-wave voltage, V_B is the DC bias voltage, η is a parameter determined by the extinction ratio of the modulator $(1+\eta)/(1-\eta)$, and V_{ph} is the photodetector voltage, defined as [2]

$$V_{\mathrm{ph}} = \frac{\alpha P_0 \rho R G_A}{2}, \qquad (3)$$

where α is the insertion loss, P_0 is the input optical power, ρ is the responsivity of the photodetector, R is the impedance at the output of the detector, and G_A is the amplifier

voltage gain. The voltage V_{ph} is the voltage at the output of the amplifier when the modulator is biased with $V_B = V_\pi$ and its RF port is not connected.

Using the Jacobi–Anger expansion [13], Eq. (2) becomes

$$V_{\mathrm{out}}(t,T) = V_{\mathrm{ph}}\left\{ 1 - \eta\sin(\pi V_B/V_\pi)J_0(\pi|a_{\mathrm{in}}^{\mathrm{mod}}(T)|/V_\pi)\right.$$

$$- 2\eta\sin(\pi V_B/V_\pi)\sum_{m=1}^{\infty}(-1)^m J_{2m}(\pi|a_{\mathrm{in}}^{\mathrm{mod}}(T)|/V_\pi)$$

$$\times\cos[2m\omega_c t + 2m\phi(T)] - 2\eta\cos(\pi V_B/V_\pi)$$

$$\times\sum_{m=0}^{\infty}(-1)^m J_{2m+1}(\pi|a_{\mathrm{in}}^{\mathrm{mod}}(T)|/V_\pi)$$

$$\left.\times\cos[(2m+1)\omega_c t + (2m+1)\phi(T)]\right\}, \qquad (4)$$

where J_m is an mth order Bessel function. To explicitly separate the fast time scale t from the slow time scale T, we rewrite Eq. (4) as

$$V_{\mathrm{out}}(t,T) = \mathrm{D.C.} - \eta V_{\mathrm{ph}}\cos(\pi V_B/V_\pi)J_1(\pi|a_{\mathrm{in}}^{\mathrm{mod}}(T)|/V_\pi)$$

$$\times\exp[i\phi(T)]\exp(-i\omega_c t) + \mathrm{H.H.} + \mathrm{c.c.}, \qquad (5)$$

where D.C. denotes a time-independent term and H.H. represents higher-order harmonic terms caused by the E/O modulator nonlinearity that have carrier frequencies $m\omega_c$, where $m > 1$. In Eq. (5), the only explicit appearance of the fast time t is in the factor $\exp(-i\omega_c t)$.

The modulator nonlinearity is responsible for the higher-harmonic components in Eqs. (4) and (5), centered around angular frequencies $m\omega_c$ with $m > 1$, where m is an integer. In experiments, the bandwidth of the RF filter, Γ, as well as the bandwidth of the electrical amplifier, which are of the order of tens of megahertz, are significantly narrower than the carrier angular frequency ω_c, i.e., $\Gamma \ll \omega_c$. Hence, we may neglect higher-order harmonic terms in our model. Only the cavity modes that are centered at the carrier angular frequency ω_c ($m=1$) will propagate through the cavity, while the other cavity modes are filtered out. In [2], this neglect is referred to as a quasi-linear approximation. The effect of the higher-order modes on the amplifier saturation is similarly neglected.

Using the quasi-linear approximation, and including the effects of the E/O modulator, the photodetector, and the RF amplifier on the signal amplitude, we obtain the phasor of the RF amplifier output voltage $a_{\mathrm{out}}^{\mathrm{amp}}(T)$,

$$a_{\mathrm{out}}^{\mathrm{amp}}(T) = -2\eta\cos(\pi V_B/V_\pi)V_{\mathrm{ph}}J_1(\pi|a_{\mathrm{in}}^{\mathrm{mod}}(T)|/V_\pi)\exp[i\phi(T)].$$
$$(6)$$

We note that in contrast to [2] our model does not require the signal in the cavity to be a sinusoidal signal with a constant amplitude. We allow the amplitude $a(T)$ and the phase $\phi(T)$ to vary on a slow time scale. In fact, we will demonstrate that it is possible for the amplitude of the OEO signal to oscillate even in steady state.

We assume that the RF filter is linear. Hence, in the time domain the filter response is given by

$$a_{\text{out}}^{\text{fil}}(T)\exp(-2\pi i f_c T) = \int_{-\infty}^{T} a_{\text{in}}^{\text{fil}}(T')\exp(-2\pi i f_c T')f(T-T')\text{d}T',$$ (7)

where $a_{\text{in}}^{\text{fil}}(T)=a_{\text{out}}^{\text{amp}}(T)$ and $a_{\text{out}}^{\text{fil}}(T)$ are the phasors of the filter input and output signals, respectively; $f_c=\omega_c/2\pi$ is the carrier frequency; and $f(T)$ is the impulse response of the filter. We note that f_c is chosen arbitrarily near to the central frequency of the filter. The actual oscillation frequency is determined by the OEO dynamics and the RF filter and may not equal the carrier frequency. The filter smooths the signal in the time domain and also adds a delay to the signal. The output of the filter is affected by its input signal at a time interval that is equal to the effective duration of the filter impulse response $T_f=1/\Gamma$. Hence, the output of the filter in the time domain is determined by its input in the time interval $[T-T_f,T]$.

To calculate the filter response in the frequency domain we consider the complex amplitude $a(T)$ in a time window $[T-T_{\text{tot}},T]$ such that $T_{\text{tot}}>T_f$ and expand it as a Fourier series

$$a(T) = \sum_{k=-\infty}^{\infty} \tilde{a}(f_k)\exp(-2\pi i f_k T),$$ (8)

where $\tilde{a}(f_k)$ denote the Fourier coefficients and $f_k=k/T_{\text{tot}}$ is the frequency offset with respect to the chosen carrier frequency f_c. In the frequency domain the filter response is given by

$$\tilde{a}_{\text{out}}^{\text{fil}}(f_k) = F(f_k + f_c)\tilde{a}_{\text{in}}^{\text{fil}}(f_k),$$ (9)

where $\tilde{a}_{\text{in}}^{\text{fil}}(f_k)$ and $\tilde{a}_{\text{out}}^{\text{fil}}(f_k)$ are the Fourier coefficients of the complex amplitudes $a_{\text{in}}^{\text{fil}}(T)$ and $a_{\text{out}}^{\text{fil}}(T)$, respectively, and $F(f')$ is the Fourier transform of the function $f(T)$,

$$F(f') = \int_{-\infty}^{\infty} f(T)\exp(2\pi i f' T)\text{d}f'.$$ (10)

In our simulations we assumed a filter with a Lorenzian line shape,

$$F(f_k + f_c) = \frac{i\Gamma/2}{f_k + f_c - f_0 - i\Gamma/2},$$ (11)

where Γ is the the full width at half-maximum (FWHM) of the filter transmission spectrum and f_0 is the central frequency of the filter. In the time domain the filter impulse response is given by

$$f(T) = \pi\Gamma\,\exp[-2\pi i(f_0 + i\Gamma/2)T]u(T),$$ (12)

where $u(T)$ is the Heaviside step function.

A. Simulation Model
As noted in the Introduction, the principal difficulty that prevents a straightforward simulation of the OEO is the existence of three different frequency scales. Due to the difference between the highest and the lowest time scales a straightforward implementation of the OEO simulation is impractical as one cannot follow fluctuations that occur at a millisecond time scale while resolving gigahertz oscillations. Our simulation model was developed in order to overcome this difficulty.

In our model we calculate the complex amplitude of the signal inside the OEO on each round trip. The voltage envelope $a_{\text{in}}^{\text{fil}}(T)$ is defined at the input of the filter. We define the complex amplitude function $a^l(T)$ as the complex amplitude $a_{\text{in}}^{\text{fil}}(T)$ given in a time interval of $(l-1)\tau \leq T < l\tau$ where l is an integer, $\tau=nL/c$ is the round-trip time added by the fiber, L is the fiber length, and n is the effective refractive index of the fiber. We start the simulation assuming that $a^l(T)=0$ $(l\leq 0)$, where l is an index that counts the number of round trips that the signal makes after the OEO is switched on. At each iteration we calculate the propagation of the signal through the filter, the detector, and the modulator in a single round trip. After each round trip we add noise due to the amplifier, the detector, and the laser.

We assume that the effective duration of the filter impulse response is shorter than the delay of the cavity fiber τ, i.e., $\Gamma\tau \gg 1$. We use the functions $a^{l-1}(T)$ and $a^l(T)$ to obtain the complex amplitude of the filter input that is defined over the finite time interval $(l-2)\tau \leq T < l\tau$

$$a_{\text{in},2\tau}^l(T) = \begin{cases} a^{l-1}(T) & \text{for } (l-2)\tau \leq T < (l-1)\tau \\ a^l(T) & \text{for } (l-1)\tau \leq T < l\tau \end{cases}.$$ (13)

We calculate the complex amplitude of the filter output $a_{\text{out},2\tau}^l$ using the convolution of $a_{\text{in},2\tau}^l$ and the filter impulse response as described in Eq. (7). The next round-trip complex amplitude is given by $a^{l+1}(T)=a_{\text{out},2\tau}^l(T-\tau)$ and is defined for $l\tau \leq T < (l+1)\tau$. The output signal of the filter is used as an input to the modulator. The modulator and the detector response are then calculated using Eq. (6).

There are several effects that contribute to the noise in the OEO: thermal noise in the amplifier, shot noise in the detector, and intensity noise of the laser [14]. The total noise in our system is modeled as a single white noise source that is injected into the input of the amplifier in the frequency domain. The noise is added after each round trip in the oscillator using the relationship

$$\tilde{a}_{\text{out}}^{l,\text{amp}}(f) = G_A[\tilde{a}_{\text{in}}^{l,\text{amp}}(f) + \tilde{w}^l(f)],$$ (14)

where $\tilde{a}_{\text{in}}^{l,\text{amp}}(f)$ and $\tilde{a}_{\text{out}}^{l,\text{amp}}(f)$ are the Fourier coefficients of the complex amplitude of the lth round trip at the input and output of the amplifier, respectively, and $\tilde{w}^l(f)$ denotes white Gaussian noise with a single-sideband power spectral density ρ_N that is added after each round trip [15].

Before recording any data we propagated the signal in the OEO for $N_{\text{RT}}=2000$ iterations, where N_{RT} is the number of iterations that it takes for the signal to reach a steady state. At $T_0=N_{\text{RT}}\tau$ we calculated and stored the voltage amplitude $a_{M\tau}(T)$ over M round trips of the simulation. We have validated that the calculated phase noise spectrum did not depend on T_0 as long as $T_0>N_{\text{RT}}\tau$.

B. Radio Frequency Spectrum and Phase Noise Calculation
To determine the low-frequency components of the RF spectrum in the region of 100 Hz–100 kHz we used the voltage amplitude $a_{M\tau}(T)$, defined for $T_0<T<T_0+M\tau$. We define the discrete Fourier transform of $a_{M\tau}(T)$ as

$$\tilde{a}_{M\tau}(f) \triangleq \mathcal{F}_{M\tau}[a(T)] = \frac{1}{M\tau} \int_0^{M\tau} a_{M\tau}(T + T_0)\exp(2\pi i f T)\mathrm{d}T.$$

$$(15)$$

The calculation requires the storage of the envelope function $a_{M\tau}$ accumulated over M iterations. The lowest frequency that can be resolved using Eq. (15) is of the order of $1/M\tau$.

The quality of an OEO is determined by its phase noise. When the filter bandwidth is wide compared to the cavity mode spacing, the OEO may operate in one of several different cavity modes. Unless the oscillation frequency is exactly equal to the chosen carrier frequency f_c, the phase $\phi(T)$ depends linearly on time. To calculate the phase noise in these cases we subtract the linear phase change from the time-dependent phase. We also subtract the time-averaged phase when calculating the phase noise, leaving only quadratic and higher-order dependence on time. The phase noise is expressed as the power spectral density of the phase, $S_\phi(f)$, which is equal to the Fourier transform of the autocorrelation function of the phase $\phi(T)$ [16].

In each simulation, we calculated the low-frequency components of the phase noise using the relation

$$\tilde{\phi}_{M\tau}(f) = \mathcal{F}_{M\tau}[\phi(T)].$$

$$(16)$$

The phase spectrum calculated over a time interval of $M\tau$ is found by dividing the spectral power of the phase by the frequency resolution $\delta f' = 1/M\tau$,

$$S_\phi^{M\tau}(f) = |\tilde{\phi}_{M\tau}(f)|^2/\delta f'.$$

$$(17)$$

We note that when $M \to \infty$, the expectation value of the phase spectrum, $S_\phi^{M\tau}(f)$, approaches the power spectral density of the phase, $S_\phi(f)$. However, the phase spectrum contains noise that changes from one simulation to the next, just as is the case in experiments. In Subsection 3.A we show, by fitting a line to the curve that gives the dependence of the logarithm of the phase spectral power on the logarithm of the frequency, that it is possible to estimate the function $S_\phi(f)$ accurately when M is as low as 5000. We have also verified, as discussed in Subsection 3.A that the phase noise in OEOs may be obtained to a very high accuracy by calculating the RF spectrum $S_{RF}^{M\tau}(f)$,

$$S_\phi^{M\tau}(f) \cong S_{RF}^{M\tau}(f) = \frac{|\mathcal{F}_{M\tau}[a(T)]|^2}{2RP_{osc}\delta f'},$$

$$(18)$$

where $P_{osc} = |\tilde{a}(f=0)|^2/2R$ is the carrier power. The RF spectrum is approximately equal to the phase noise spectrum over a wide frequency range in OEOs since the amplitude noise is negligible and the phase fluctuation is much smaller than unity.

3. SIMULATION RESULTS

In this section, we describe our principal simulation results. We have implemented our model by discretizing the function $a^l(T)$ using an array containing $N = 200$ points, which induces a finite resolution time $\delta T = \tau/N$. The round-trip time in the cavity was set to $\tau \cong 0.28$ μs. As a result, the frequency resolution, $\delta f = 1/\tau$, was about δf

$\cong 3.5$ MHz and the simulation bandwidth, $\Delta f = 1/\delta T$, was about $\Delta f \cong 700$ MHz. We note that the number of points, N, should be chosen sufficiently high to ensure that the simulation bandwidth will be significantly broader than the RF filter FWHM bandwidth.

At each iteration N mutually independent noise variables $\tilde{w}_i^l$ were added to the signal $\tilde{a}^l(f_i)$, $i = 1, \ldots, N$. The variance of the noise variables is set by the relation $\langle |\tilde{w}_i^l|^2 \rangle / 2R = \rho_N \delta f$, where ρ_N is the noise spectral density and $R = 50$ Ω is the input resistance of the amplifier. Assuming a complex Gaussian distribution, each of the real and the imaginary parts of the independent noise variables was normally distributed with a variance $A_{NL}^2/2$, where

$$A_{NL} = \sqrt{2\rho_N \delta f R}.$$

$$(19)$$

The power spectral density of the noise in our simulation was taken to be $\rho_N = 10^{-17}$ mW/Hz unless otherwise specified. This value is consistent with the power spectral density used in [2]. We note that the results of the simulation were not sensitive to the exact distribution of the noise variables. We verified that all of the simulation results in this paper are not changed when we assume an input noise with a uniform phase and a uniform amplitude distribution.

Each simulation models the propagation of light in an OEO through 12,000 cycles. The simulation parameters, unless otherwise specified, were chosen as follows: filter width $\Gamma = 20$ MHz, average oscillation power at the output of the amplifier $P_{osc} = 30$ mW, half-wave voltage of the modulator $V_\pi = 3.14$ V, bias voltage $V_B = 3.14$ V, and a voltage gain of $G_A = 7.5$. The fiber length corresponding to a loop delay of 0.28 μs was equal to 56 m. The values of these parameters are similar to those used in the theoretical analysis and in the experimental results given in [2]. We note that in a modern OEO the loop length is of the order of a few kilometers and that mode hopping may be prevented by using a multiloop OEO [4,5,9,17]. An important parameter that determines the OEO behavior is the small-signal open-loop gain, G_S, given by [2]

$$G_S = -\frac{\eta\pi V_{ph}}{V_\pi}\cos(\pi V_B V_\pi),$$

$$(20)$$

which can be either positive or negative, depending on the modulator bias voltage, V_B. In our simulation, unless otherwise specified, the small-signal open-loop gain is set equal to $G_S = 1.5$.

The run-time duration of the simulation using a personal computer, an IBM T43 with a CPU speed of 1.86 GHz and 1 GB of RAM, was of the order of only a few minutes. To obtain the noise components at low frequencies of the order of 100 Hz–100 kHz, the voltage amplitude $a^l(T)$ was accumulated over the last $M = 10,000$ round trips of the simulation. This number of round trips corresponds approximately to a duration of about 3 ms.

A. Phase Noise
Figure 2 shows the phase noise as a function of the frequency offset on a logarithmic scale. The dependence of the average phase noise on the frequency is obtained by making a linear fit to the plot. Figure 2 shows that the
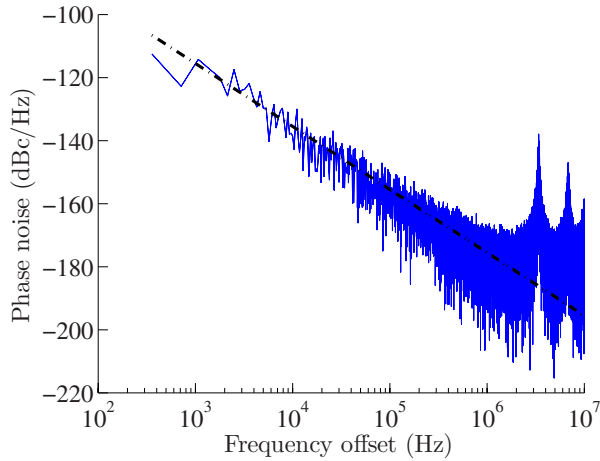
Fig. 2. (Color online) Phase noise spectral density (solid curve) as a function of the frequency offset obtained for an OEO with a loop delay of $\tau = 0.28$ μs, oscillation power of 14.77 dBm, filter bandwidth of $\Gamma = 20$ MHz, noise power spectral density of $\rho_N = 10^{-17}$ mW/Hz, small-signal open-loop gain of $G_S = 1.5$, and a voltage gain of $G_A = 7.5$. The noise was calculated over $M = 10,000$ round trips. A least-squares fit of the phase noise curve (dashed-dotted line) yields $-55.5 - 20 \log_{10}(f)$.

average phase noise power has a 20 dB per decade dependence on the frequency offset, in agreement with the theoretical and experimental results given in [2]. We note that the exact phase noise level at each frequency is different in each simulation because the noise is random. The peaks at frequencies 3.57 and 7.14 MHz correspond to the cavity modes. The ability to simulate dynamical effects allows us to calculate the fluctuations of the OEO signal due to random variations of the input noise. These fluctuations are responsible for the random variations in the phase spectrum that are visible in Fig. 2.

To check the effect of the integration time $M\tau$ on the results, we compared the phase noise that was obtained using three different values of $M\tau$. The results are shown in Fig. 3. Since the process is ergodic, the phase noise statistics and the phase noise average value at a given frequency should be independent of the finite integration time $M\tau$. However, since the frequency resolution, which is also the minimal frequency offset, is equal to $\delta f'' = 1/M\tau$, Figs. 3(a)–3(c) are slightly different. When M increases, the frequency resolution increases and the variation in the phase noise also increases. However, the average phase noise does not change.

Figure 4 demonstrates the ergodicity of the results. The noise (solid curve) was obtained by averaging the phase noise of 350 simulation results such as the one shown in Fig. 2. The result of this average is approximately equal to that obtained by making a linear least-squares fit to the phase spectrum. The least-squares fit is shown in Fig. 2 as a dashed-dotted curve. A comparison of the averaged phase noise to the RF spectral density obtained using the Yao–Maleki model [2] (dashed curve) shows that both results have the same dependence on frequency. However, the Yao–Maleki model produces a noise spectral density that is 2.5 dB higher than does our simulation model. In the Yao–Maleki model, the steady-state loop gain is set equal to 1, and the round-trip gain does not change in time. Therefore, the reduction of the amplitude noise due
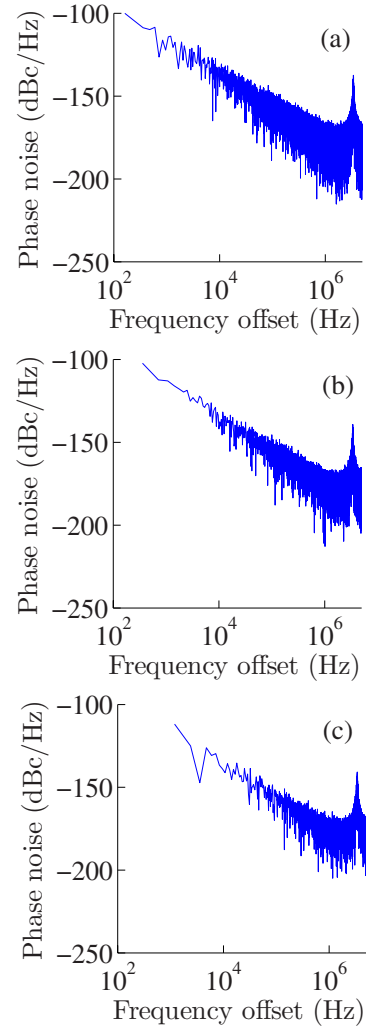

Fig. 3. (Color online) Phase noise spectral density $S_\phi(f)$ calculated for three different integration times: (a) $M\tau =$ (b) 8.4, 2.8, and (c) 0.84 ms.

to negative feedback from the fast E/O modulator response is not taken into account in the Yao–Maleki model. Our model includes this fast response.

We also verified that the RF spectral density is approximately equal to the phase noise; i.e., $S_{RF}(f) \cong S_\phi(f)$ [16]. This assumption is valid because the amplitude noise, which is suppressed by the fast response of the optical modulator, is small relative to the phase noise and because the phase fluctuation is significantly smaller than unity, $\delta\phi(T) \ll 1$. Figure 5 shows that the averaged RF spectrum is almost identical to the averaged phase spectrum in a broad frequency range. At a frequency equal to nearly half the cavity mode spacing, there is a discrepancy between $S_{RF}(f)$ and $S_\phi(f)$. This discrepancy is due to amplitude noise, which has a value of about -170 dB and is not strongly dependent on the frequency. However, phase noise dominates when the frequency offset becomes smaller than the cavity mode spacing, and at a frequency offset less than about $0.1/\tau$ the difference between S_{RF} and S_ϕ is negligible.

The Yao–Maleki model [2] predicts that when the angular frequency is significantly lower than the cavity mode spacing, i.e., when $2\pi f\tau \ll 1$, and when the frequency off-
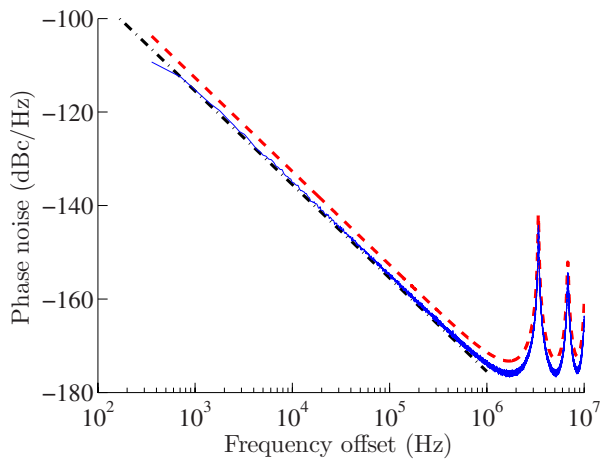
Fig. 4. (Color online) Comparison between the phase noise spectral density, $S_\phi(f)$, calculated by averaging the phase noise over 350 simulations (solid curve) and by performing a least-squares fit to a single simulation result that is shown in Fig. 2 (dashed-dotted line). The curves are compared to that obtained by using the Yao–Maleki model [2] (dashed curve). The approximately 2.5 dB difference is due to the neglect in the Yao–Maleki model of the modulator's fast gain response.

set is higher than the FWHM bandwidth of the OEO signal, the dependence of the phase noise, $S_\phi(f)$, on the noise power spectral density and on the loop delay is proportional to ρ_N/τ^2. The latter dependence has been verified experimentally [2]. To verify that our simulations produce the same result, we have analyzed the dependence of the phase noise on the loop delay and on the noise power spectral density. The phase noise in the frequency range of 10 kHz–1 MHz was calculated for different cavity lengths and different input noise levels. The average phase noise was calculated for each cavity by averaging 350 runs as was done to obtain Fig. 4. The results were compared to the results of the Yao–Maleki model [2]. Figure 6 shows the phase noise of the OEO (circles) at a 30 kHz offset from the carrier as a function of loop delay. The other cavity parameters were the same as in Fig. 2. A

Fig. 6. (Color online) Phase noise spectral density of the OEO at a frequency offset of 30 kHz as a function of loop delay τ (circles) and the filter bandwidth in each case was $\Gamma = 5.6/\tau$. The least-squares fitting of the data points (solid line) is given by: $-155.4 - 20\log_{10}[\tau(\mu s)]$, which is in agreement with the results of the Yao–Maleki model (dashed line): $-152.8 - 20\log_{10}[\tau(\mu s)]$. The simulation phase noise was extracted by fitting a curve at each delay using a least-squares fit, as shown in Fig. 2. A difference between the models of approximately 2.5 dB is visible at all loop delays.

linear least-squares fit to the averaged phase spectrum (in decibels) yielded the following dependence of the phase noise on the loop delay: $-155.4 - 20\log_{10}[\tau(\mu s)]$. The dependence of the phase noise on the loop delay obtained using the results in [2] is equal to: $-152.8 - 20\log_{10}[\tau(\mu s)]$. Figure 7 shows the phase noise at a 30 kHz offset from the carrier as a function of the noise power spectral density. The dependence of the phase noise on the noise power spectral density is equal to $25.62 + \rho_N(\mathrm{dBm/Hz})$. The Yao–Maleki model [2] yields the dependence $28.25 + \rho_N(\mathrm{dBm/Hz})$. We note that in the Yao–Maleki model and in our studies the filter bandwidth $\Gamma = 20$ MHz is taken into account.
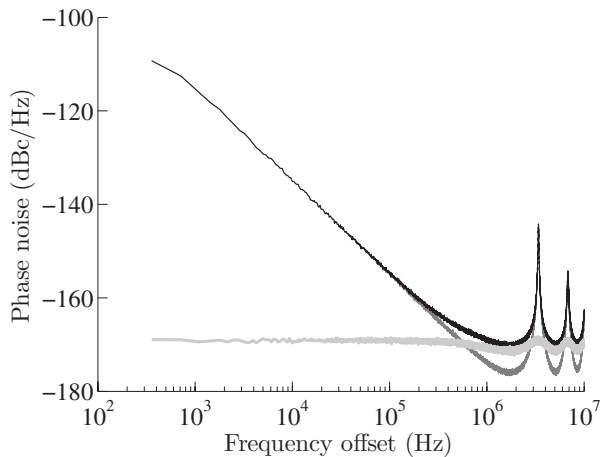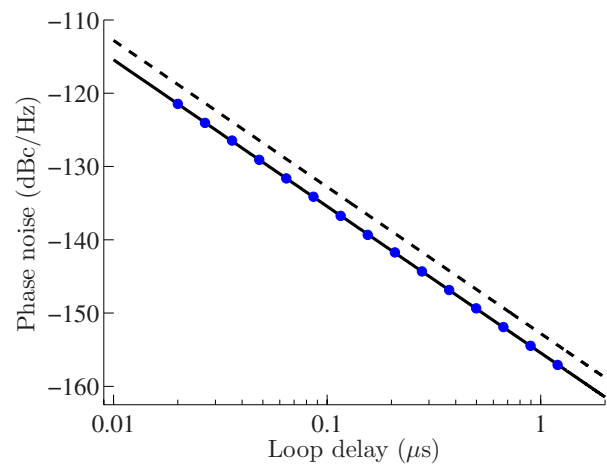

Fig. 5. Comparison between a phase noise spectral density $S_\phi(f)$ (dark gray curve), amplitude noise (light gray curve), and the complete RF spectrum $S_{\mathrm{RF}}(f)$ (black curve), which are calculated by averaging the noise over 350 simulations. The comparison justifies the approximation that $S_{\mathrm{RF}}(f) \cong S_\phi(f)$ for a wide frequency range in which the amplitude noise is negligible relative to the phase noise.
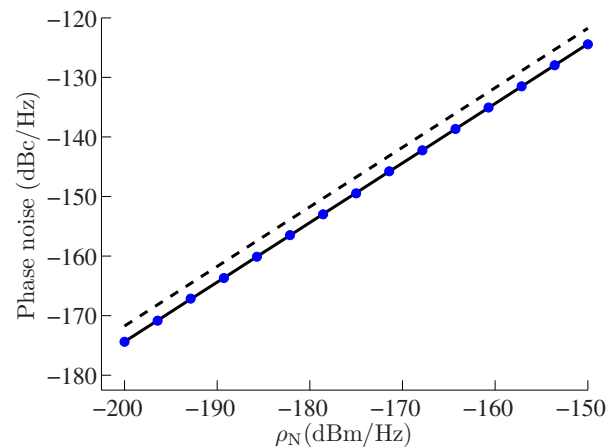

Fig. 7. (Color online) Comparison between phase noise spectral density at a frequency offset 30 kHz offset as a function of the spectral noise density power calculated by using the Yao–Maleki model (dashed line) and by using our simulation (circles). The least-squares fit of the simulation data points (solid line), given by $25.62 + \rho_N(\mathrm{dBm/Hz})$, is compared to the result of the Yao–Maleki model (dashed line): $28.25 + \rho_N(\mathrm{dBm/Hz})$.

The dependence of the phase noise on the loop delay and on the frequency offset obtained in our simulation is the same as that obtained theoretically and experimentally in [2]. Our simulation, as well as the previous result, give a 20 dB per decade dependence of the phase noise on the frequency offset and on the loop delay. As noted previously, the Yao–Maleki model yields a power spectral density of the phase that is 2.5 dB higher than our simulation model produces. However, when the small-signal open-loop gain G_S approaches 1, the amplitude noise becomes stronger at lower frequencies. Therefore, in a broad frequency range the disagreement between the two models vanishes. For example, for $G_S = 1.05$ the amplitude noise power becomes similar to the phase noise above a frequency offset of $0.01/\tau$. Hence, at a frequency range $f > 0.01/\tau$ the results of our model and the Yao–Maleki model in [2] become approximately equal.

B. Cavity Mode Competition and Selection at Start-Up in the Optoelectronic Oscillator

In the Yao–Maleki model it is assumed that only one cavity mode has a small-signal open-loop gain that is larger than unity and therefore only one cavity mode is allowed to oscillate. Since the cavity length of OEOs is long, the cavity mode spacing is usually far smaller than the bandwidth of the filter, so that several cavity modes may have a small-signal open-loop gain greater than 1. All such modes can potentially oscillate and hence the OEO can oscillate in one of several cavity modes. Our simulation model includes many cavity modes. The noise that is present when the OEO is turned on determines the specific cavity mode that oscillates once the OEO reaches steady state. After one of the cavity modes starts oscillating, the small signal gain of the other cavity modes decreases due to gain saturation of the modulator. Large amounts of noise can in principle lead to mode hopping, but at the noise power levels in our simulations, which correspond to typical experimental power levels, we have not observed that to date. This result implies that the experimentally observed mode hopping [12] is not due to Gaussian white noise, but is due to other environmentally driven noise sources.

Figure 8 shows the spectrum and the time dependence of the OEO signal envelope when the OEO can oscillate in different cavity modes. The round-trip time was set equal to $\tau = 2$ μs and the chosen carrier frequency was equal to the central frequency of the RF filter $f_c = f_0$. The normalized frequency $f\tau$ is the offset frequency with respect to the chosen carrier frequency f_c that is normalized by the cavity mode spacing. Figure 9(a) shows the probability density function (PDF) of the normalized oscillation frequency. The OEO can oscillate in five different normalized oscillating frequencies, each of which corresponds to a different cavity mode. The standard deviation of the normalized oscillating frequency, σ_{mod}, is equal to $\sigma_{\mathrm{mod}} = 0.96$. The standard deviation of the normalized oscillating frequency distribution depends on the ratio between the RF filter bandwidth and the cavity mode spacing, $\Gamma\tau$. Figure 9(b) shows the standard deviation of the normalized oscillating frequency as a function of this ratio. In our simulations we varied the round-trip time while keeping the RF filter bandwidth constant. We did not observe that
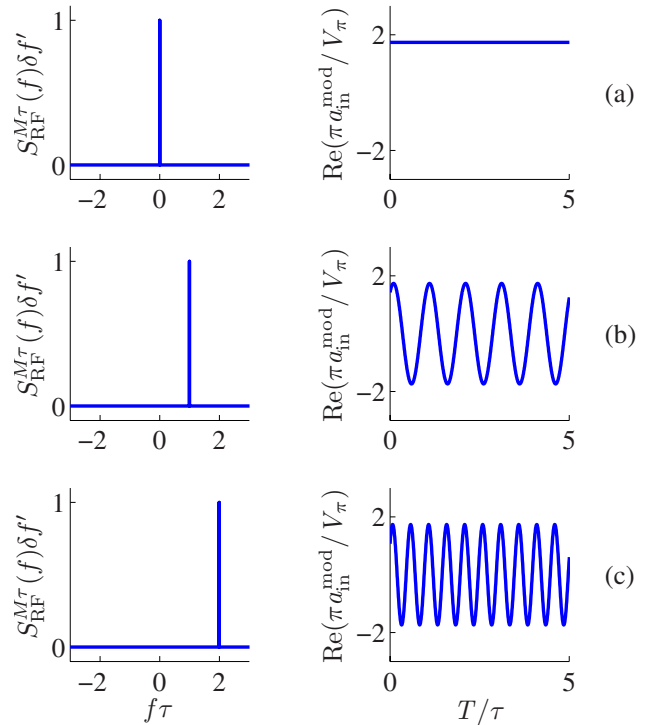

Fig. 8. (Color online) Oscillation in one of several oscillating cavity modes where the RF filter bandwidth Γ is equal to 20 MHz and the round-trip time τ is equal to 2 μs. (a) The RF spectrum (left) and the real part of the amplitude (right) when the steady-state cavity mode has a frequency f_c. (b) The RF spectrum (left) and the real part of the amplitude (right) when the cavity mode that oscillates in steady state has a frequency $f_c + 1/\tau$. (c) The RF spectrum (left) and the real part of the amplitude (right) when the steady-state cavity mode has a frequency $f_c + 2/\tau$.

the PDF of the normalized frequency was dependent on the power spectral density of the injected white noise.

C. Nonstationary Steady-State Behavior

We have studied the dependence of the OEO oscillation amplitude on the small-signal open-loop gain G_S, defined in Eq. (20), and on the filter bandwidth Γ. We have found that when $G_S > 2.31$, amplitude oscillations occurs. These amplitude oscillations cannot be studied within the context of the Yao–Maleki model, which assumes that in steady-state the oscillations do not change in time. We also find that when $G_S \gtrsim 2.9$, amplitude oscillations at more than one frequency appear, and the temporal evolution becomes aperiodic. Finally, we find that when the filter bandwidth Γ is smaller than approximately $2/\tau$, the amplitude oscillations are suppressed. To suppress oscillations at more than one frequency, the required filter bandwidth should be narrower than $2/\tau$. Chembo *et al.* [11] have experimentally observed amplitude oscillations in the OEO, and they described this effect using a simple delay-differential equation. However, the model that was used to derive the threshold for amplitude oscillation does not include the effect of the RF filter and its transmission profile. Hence, it cannot explain the suppression of the amplitude oscillation that is observed in our simulations when the filter bandwidth narrows.

In Fig. 10 we show the time dependence of the amplitude and phase for $G_S = 1.5$. No amplitude oscillations are
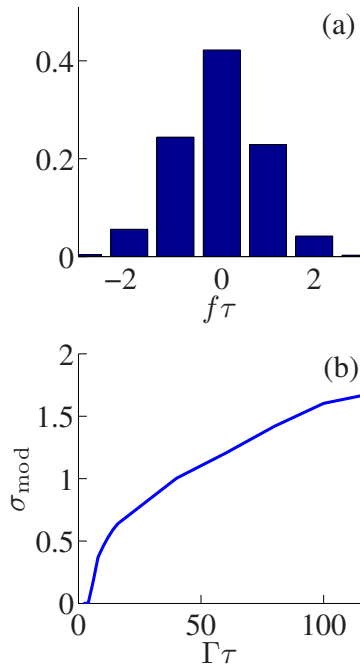
Fig. 9.   (Color online) (a) Probability density function of the normalized oscillating frequency when $\Gamma\tau=40$. The normalized oscillating frequency is distributed with a standard deviation of $\sigma_{\mathrm{mod}}=0.96$. (b) The standard deviation of the normalized oscillating frequency distribution as a function of $\Gamma\tau$.

observed. Figure 11 shows the amplitude of the OEO as a function of time for $G_S=2.4$, which is above the threshold $G_S=2.31$ and, in this case, amplitude oscillations with a period of 2τ are observed. The change in the amplitude of the output signal is about 0.15 of the average amplitude. Figure 12 shows how the minimum and the maximum
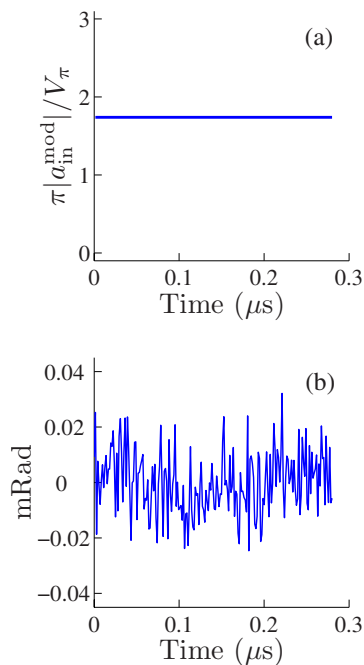

Fig. 10.   (Color online) (a) Normalized amplitude and (b) phase noise obtained for a small-signal open-loop gain $G_S=1.5$. The steady-state amplitude does not depend on time and is equal to $1.75V_\pi/\pi$. The other OEO parameters are the same as in Fig. 2.
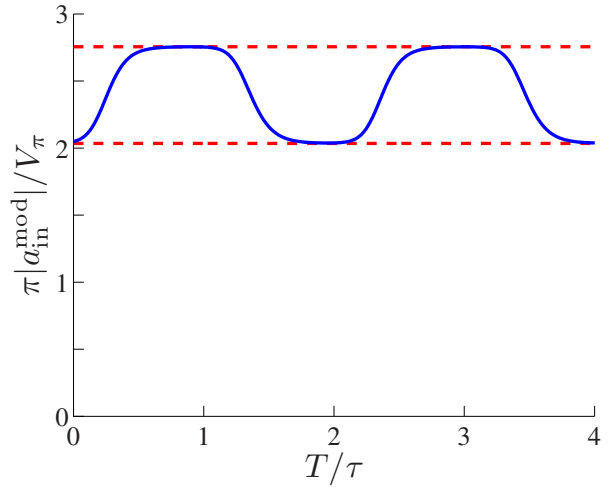

Fig. 11.   (Color online) Normalized amplitude obtained for a small-signal open-loop gain $G_S=2.4$ (solid curve). The normalized amplitude changes between 2.035 and 2.755 (dashed lines) as predicted by our threshold condition. The other OEO parameters are the same as in Fig. 2.

amplitudes depend on the filter bandwidth, and, as stated previously, temporal amplitude oscillations are only observed when $\Gamma>2/\tau$.

When the small-signal open-loop gain is increased to $G_S\gtrsim2.71$ an amplitude oscillation with a period of 4τ is obtained. Figure 13 shows a 4τ-periodic amplitude oscillation that is obtained for $G_S=2.75$.

When the small-signal open-loop gain is further increased to $G_S\gtrsim2.9$, oscillations at two or more frequencies are observed, as shown in Fig. 14, although the change in the phase remains small. We define a time-averaged oscillation power $P_{\mathrm{avg}}(T)$,

$$P_{\mathrm{avg}}(T)=\frac{1}{T_P}\int_{-T_P/2}^{T_P/2}\frac{|a(T-T')|^2}{2R}\mathrm{d}T', \qquad (21)$$

where T_P is the time over which the average power is calculated. We have found that although the amplitude in
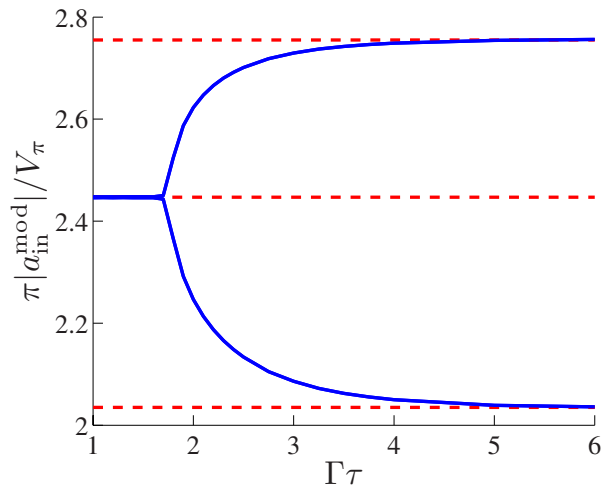

Fig. 12.   (Color online) Minimum and maximum amplitude obtained for a small-signal open-loop gain $G_S=2.4$ as a function of the filter bandwidth. The other OEO parameters and the pulse shape are the same as in Fig. 2. The dashed lines show our threshold condition and the minimum and maximum amplitude excursions.
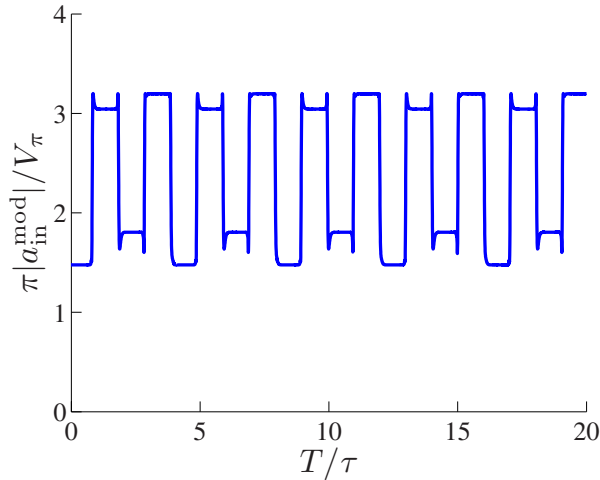
Fig. 13. (Color online) Normalized amplitude obtained for a small-signal open-loop gain $G_S = 2.75$. Amplitude oscillations with a period of 4τ are obtained as predicted by our threshold condition. The other OEO parameters are the same as in Fig. 2.

Fig. 14(a) varies, its time-averaged oscillation power $P_{\text{avg}}(T)$ approaches a constant value when $T_P \geq 5\tau$ as shown in Fig. 14(a). In [2] the amplitude of the oscillation was calculated for a small-signal open-loop gain G_S that was varied from 1 to 4. The result was verified experimentally only when the gain varied between 1 and approximately 2 [2]. Figure 15 compares the dependence of the time-averaged power on the small-signal openloop gain that was obtained using our simulation to that calculated by using the Yao–Maleki model [2]. Our result shows that
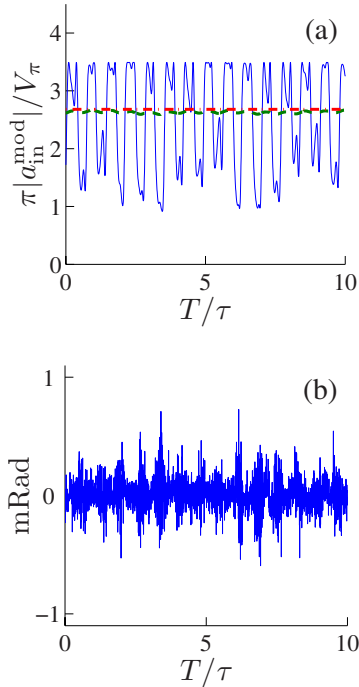

Fig. 14. (Color online) (a) Amplitude and (b) phase obtained for a small-signal open-loop gain $G_S = 3$. The dashed line in (a) gives the amplitude derived from the averaged power $[2RP_{\text{avg}}(T)]^{1/2}$. The power is averaged over a time duration of $T_P = 5\tau$ (dashed curve) and is compared to the result of the Yao–Maleki model $2.68V_\pi/\pi$ (dashed-dotted line). The simulation parameters are the same as in Fig. 2.
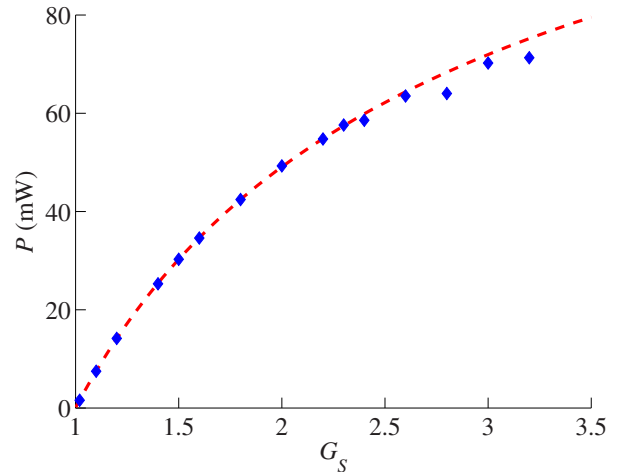

Fig. 15. (Color online) Dependence of the time-averaged oscillation power as a function of the small-signal open-loop gain calculated in the simulations (diamonds) and compared to the power from the Yao–Maleki model [2] (dashed curve). The averaging time was 10τ. Good agreement is obtained between the results although the assumption in the Yao–Maleki model that the amplitude does not change in time is not valid for $G_S > 2.31$.

despite the amplitude oscillations when $G_S > 2.31$, the average OEO power is still consistent with the Yao–Maleki model.

The oscillation thresholds that we observe in our simulations and that were found by Chembo *et al.* [11] may be derived using a simple physical argument. The small-signal open-loop gain must be greater than unity in order for the OEO to oscillate [2]. The nonlinearity of the E/O modulator limits the amplitude of the oscillating cavity mode. To obtain a steady-state solution with a time-independent amplitude, the average loop gain should be slightly less than one [2]. Therefore, we assume that the round-trip gain equals unity. Using Eq. (6), we find

$$V_{\text{out}} = G(|a_{\text{in}}^{\text{fil}}|)|a_{\text{in}}^{\text{fil}}|\cos(\omega_c t + \phi),\qquad(22)$$

where the round-trip gain coefficient $G(|a_{\text{in}}^{\text{fil}}|)$ is given by

$$G(|a_{\text{in}}^{\text{fil}}|) = 2G_S \frac{V_\pi}{\pi|a_{\text{in}}^{\text{fil}}|} J_1(\pi|a_{\text{in}}^{\text{fil}}|V_\pi).\qquad(23)$$

According to Eqs. (22) and (23), the relation between the oscillation amplitude in two sequential round trips l and $l+1$ that is needed to obtain a time-independent amplitude is

$$\pi|a^{l+1}(T)|V_\pi = 2G_S \cdot J_1(\pi|a^l(T)|V_\pi).\qquad(24)$$

We define a normalized amplitude $x^l = \pi|a^l|/V_\pi$ and rewrite Eq. (24) as

$$x^l = x^{l+1} = f_{G_S}(x^l),\qquad(25)$$

where

$$f_{G_S}(x) = 2G_S \cdot J_1(x).\qquad(26)$$

Equation (25) has a nontrivial solution only for $G_S > 1$. This solution corresponds to an oscillation with a time-independent amplitude. This threshold is the same as obtained in [2].

However, in addition to the condition of a constant amplitude solution that was analyzed in the Yao–Maleki model, other steady-state conditions may be fulfilled as well. For example, the oscillation amplitude may repeat itself after two round trips, in which case

$$x^l = x^{l+2} = f_{G_S}[f_{G_S}(x^l)] = f_{G_S}^2(x^l). \qquad (27)$$

Equation (27) has a solution only for $G_S > 2.31$. The result that was shown in Fig. 11 demonstrates an amplitude oscillation in time that satisfies the condition in Eq. (27). The small-signal open-loop gain in this figure is equal to $G_S = 2.4$. We have verified that the OEO oscillates when $G_S > 2.31$, as predicted by our threshold condition. Figure 12 shows that a narrowband filter causes the generation of a time-independent amplitude. The normalized amplitude is in agreement with the solution of Eq. (25); $x = 2.447$. For a broad bandwidth filter the minimum and the maximum normalized amplitudes approach the solutions of Eq. (27), $x_{\min} = 2.035$ and $x_{\max} = 2.755$ (dashed lines in Fig. 12). When $G_S \gtrsim 2.71$ a solution for the equation $x^l = x^{l+4}$ is obtained, which results in an amplitude oscillation with a periodicity of 4τ. Figure 13 demonstrates such an amplitude oscillation, which is obtained for $G_S = 2.75$. When G_S is further increased, more solutions can arise in which $x^l = x^{l+m}$. In this case two or more frequencies may be present, leading to an aperiodic evolution as we already noted. However, as the number of different oscillation frequencies increases, the rate of change of the amplitude becomes increasingly rapid, and the assumption that the filter does not affect the oscillation, which we used to derive the threshold condition, becomes invalid. In practice, one should operate the OEO below the threshold at which amplitude oscillations set in.

4. CONCLUSIONS

We have developed a comprehensive simulation model to quantitatively study dynamic effects in OEOs. Although the OEO is characterized by three widely separated time scales, our model does not require either long run times or a large amount of memory storage. Our model generalizes the previously published model of Yao and Maleki [1] in order to take into account dynamic effects in OEOs. It includes all of the physical effects in the Yao–Maleki model as well as other physical effects that are needed to calculate important features of the OEO dynamics, such as the impact of the fast response time of the modulator on the phase noise spectral density, the cavity mode competition during the OEO start-up, and amplitude oscillations in steady state. Since our model includes all of the physical effects that are in the Yao–Maleki model, both models accurately describe the dependence of the phase noise on the cavity length, the oscillating power, and the offset frequency. These features were verified in the previous experiments of Yao and Maleki [1].

A discrepancy of 2 to 3 dB in the absolute value of the phase noise was found between the two models when the small-signal open-loop gain is greater than about 1.5. This discrepancy, which does not contradict the previously published experimental results of Yao and Maleki [1], is mainly due to the suppression of the amplitude noise that is a consequence of the fast response time of the modulator. This important effect is not taken into account in the Yao–Maleki model. Therefore, the magnitude of the RF spectrum calculated by the Yao–Maleki model is almost 3 dB too high. When the small-signal open-loop gain is close to unity, the effect of the modulator on the amplitude noise is small, and both models give approximately the same absolute noise. Modeling this dynamical effect also enables us to calculate fluctuations in the OEO signal due to random variations of the input noise. These fluctuations result in random variations in the spectrum that are obtained in our model.

With our simulation model we are able to observe cavity mode competition during the OEO start-up as well as temporal amplitude oscillations in steady state. In practice these effects can degrade the performance of OEOs if the OEO parameters are not correctly chosen. Hence, it is important to indicate when these effects are present and how they may be suppressed. When the filter bandwidth is wide enough, the OEO can oscillate in one of several cavity modes. The cavity mode that wins the mode competition and oscillates in steady state is determined by the noise that is present when the OEO is turned on.

Temporal amplitude oscillations are observed when the small-signal open-loop gain is greater than 2.31. Our model yields a threshold condition for this mode of operation based on simple physical considerations. When the small-signal open-loop gain is further increased beyond 2.9, two or more oscillation frequencies appear and the amplitude oscillation becomes aperiodic. We show that these temporal amplitude oscillations can be suppressed by using a sufficiently narrow filter.

The simulation model that we have created can be extended to include a variety of efects that are important in practice. These include fiber-length-independent flicker noise in the amplifiers and environmentally driven flicker noise that depends on the fiber length. This model can be extended to examine the impact of different amplifier and modulator designs, investigate the source of experimentally observed mode hopping and determine the requirements to suppress it, and to investigate a variety of dual-loop configurations.

ACKNOWLEDGMENT

REFERENCES

1. X. S. Yao and L. Maleki, "Converting light into spectrally pure microwave oscillation," Opt. Lett. **21**, 483–485 (1996).
2. X. S. Yao and L. Maleki, "Optoelectronic microwave oscillator," J. Opt. Soc. Am. A **13**, 1725–1735 (1996).
3. X. S. Yao and L. Maleki, "Optoelectronic oscillator for photonic systems," IEEE J. Quantum Electron. **32**, 1141–1149 (1996).
4. X. S. Yao and L. Maleki, "Dual microwave and optical oscillator," Opt. Lett. **22**, 1867–1869 (1997).
5. X. S. Yao and L. Maleki, "Multi-loop optoelectronic oscillator," IEEE J. Quantum Electron. **36**, 79–84 (2000).
6. D. Dahan, E. Shumakher, and G. Eisenstein, "Self-starting ultralow-jitter pulse source based on coupled optoelectronic

oscillators with an intracavity fiber parametric amplifier," Opt. Lett. **30**, 1623–1625 (2005).

7. N. Yu, E. Salik, and L. Maleki, "Ultralow-noise mode-locked laser with coupled opto-electronic oscillator conguration," Opt. Lett. **30**, 1231–1233 (2005).

8. W. Zhou, S. Weiss, and C. Fazi, "Developing RF-photonics components for the army's future combat systems," in *Proceedings of the 25th Army Science Conference* (2004), paper NO-02 (Report A231334, available at http://www.stormingmedia.us/23/2313/A231334.html).

9. W. Zhou and G. Blasche, "Injection-locked dual opto-electronic oscillator with ultra-low phase noise and ultra-low spurious level," IEEE Trans. Microwave Theory Tech. **53**, 929–933 (2005).

10. M. C. Li, "A high precision Doppler radar based on optical fiber delay loops," IEEE Trans. Antennas Propag. **52**, 3319–3328 (2004).

11. Y. K. Chembo, L. Larger, H. Tavernier, R. Bendoula, E. Rubiola, and P. Colet, "Dynamic instabilities of microwaves generated with optoelectronic oscillators," Opt. Lett. **32**, 2571–2573 (2007).

12. D. Eliyahu, K. Sariri, M. Kamran, and M. Tokhmakhian, "Improving short and long term frequency stability of the opto-electronic oscillator," in *Proceedings of the IEEE International Frequency Control Symposium* (IEEE, 2002), pp. 580–583.

13. F. W. J. Olver, "Bessel functions of integer order," in *Handbook of Mathematical Functions*, M. Abramowitz and I. A. Stegan, eds. (Dover, 1972), pp. 355–434.

14. A. Yariv, *Introduction to Optical Electronics*, 2nd ed. (Holt, Rinehart and Winston, 1976).

15. G. S. Fishman, "Generating samples," in *Monte Carlo: Concepts, Algorithms, and Applications* (Springer, 1996), pp. 145–254.

16. L. S. Cutler and C. L. Searle, "Some aspects of the theory and measurement of frequency fluctuations in frequency standards," Proc. IEEE **54**, 136–154 (1966).

17. D. Eliyahu and L. Maleki, "Low phase noise and spurious level in multiloop optoelectronic oscillator," in *Proceedings of the 2003 IEEE International Frequency Control Symposium* (IEEE, 2003), pp. 405–410.